Article

Systems Engineering Approach to Modeling and Analysis of Chronic Obstructive Pulmonary Disease Part II: Extension for Variable Metabolic Rates

Varghese Kurian, Michelle Gee, Sean Farrington, Entao Yang, Alphonse Okossi, Lucy Chen, and Antony N. Beris*
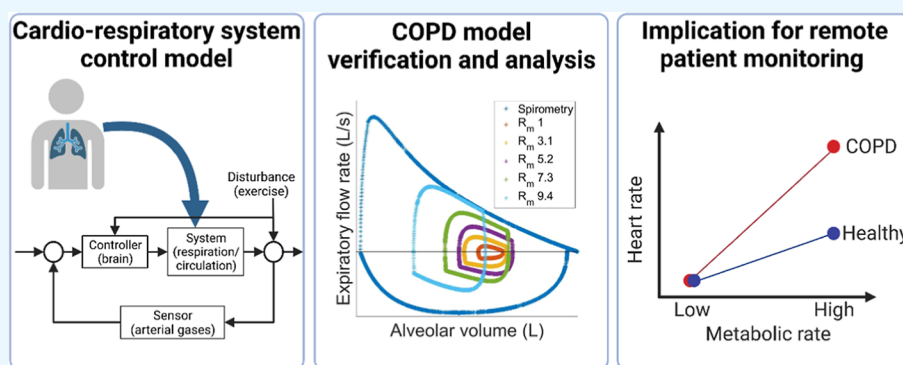
Cite This: *ACS Omega* 2024, 9, 494−508

Read Online

ACCESS | Metrics & More | Article Recommendations | SI Supporting Information

ABSTRACT: Recently, we developed a systems engineering model of the human cardiorespiratory system [Kurian et al. *ACS Omega* **2023**, *8* (23), 20524−20535. DOI: 10.1021/acsomega.3c00854] based on existing models of physiological processes and adapted it for chronic obstructive pulmonary disease (COPD)—an inflammatory lung disease with multiple manifestations and one of the leading causes of death in the world. This control engineering-based model is extended here to allow for variable metabolic rates established at different levels of physical activity. This required several changes to the original model: the model of the controller was enhanced to include the feedforward loop that is responsible for cardiorespiratory control under varying metabolic rates (activity level, characterized as metabolic equivalent of the task—R_m—and normalized to one at rest). In addition, a few refinements were made to the cardiorespiratory mechanics, primarily to introduce physiological processes that were not modeled earlier but became important at high metabolic rates. The extended model is verified by analyzing the impact of exercise ($R_m > 1$) on the cardiorespiratory system of healthy individuals. We further formally justify our previously proposed adaptation of the model for COPD patients through sensitivity analysis and refine the parameter tuning through the use of a parallel tempering stochastic global optimization method. The extended model successfully replicates experimentally observed abnormalities in COPD—the drop in arterial oxygen tension and dynamic hyperinflation under high metabolic rates—without being explicitly trained on any related data. It also supports the prospects of remote patient monitoring in COPD.

1. INTRODUCTION

Systems engineering tools—highly regarded for the unprecedented growth they have produced in manufacturing and logistics—have recently catalyzed major advancements in the healthcare industry.[1−4] Through synchronizing and exploiting the information available, these mathematical methods have found immense applications in drug discovery and development, therapeutic planning, diagnostics, pharmaceutical manufacturing, and patient management.[3,5−11] Furthermore, they are being increasingly employed to generate novel insights into the nature and function of biological systems—identifying reaction and signaling pathways in living cells, deciphering the interactions between organs and organ systems, homeostasis within the organism, or sometimes even multiscale biological

phenomena.[12−17] In this work, combining a systems engineering model of the human cardiorespiratory system with formal methods for sensitivity analysis and parameter estimation, we seek to improve our understanding of a widely prevalent condition called chronic obstructive pulmonary disease (COPD).
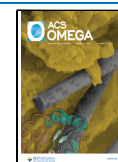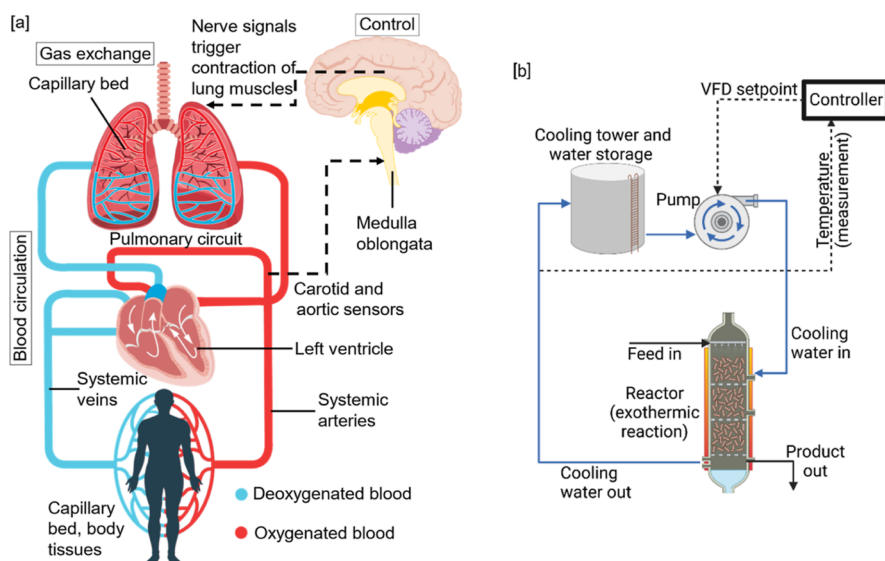
Figure 1. (a) Schematic of the cardiorespiratory systems that shows ventilation, circulation, and their control. Adapted with permission from ref 24. Copyright 2023, the authors. Image of the cardiorespiratory system: istockphoto.com. Copyright 2022, istockphoto.com/colematt. Image of the brain: adapted with permission from Cancer Research UK; obtained via Wikimedia Commons. Copyright 2014, Cancer Research UK. (b) Schematic of an industrial control system for regulating the flow of cooling water to an exothermic reactor that shows substantial resemblance to cardiorespiratory control. VFD—variable frequency drive.

COPD is an inflammatory lung disease characterized by persistent airflow obstruction that is severe enough to interfere with normal breathing function. The airflow limitation is a result of bronchial or alveolar abnormalities or a combination of them, usually caused by significant exposure to irritating gases such as wood or cigarette smoke.[18,19] The disease has an estimated global prevalence of over 10% (in the population aged ≥40 years) and is the third leading cause of death worldwide.[20] Consequently, the medical expenditures attributed to COPD are huge—the direct cost in the US alone is projected to approach $40 billion per year in the next few years, with similar expenses in the EU.[19] At present, several impediments exist to recognizing and assessing COPD efficiently, including the globally prevalent underdiagnosis, the limitations on differentiating COPD types, and the inability to accurately predict and modify the course of the disease.[21−23]

COPD is an umbrella term grouping together multiple manifestations of respiratory impairment occurring in varying severity and combinations. Among the different COPD symptoms, small airway disease and emphysema appear to be the most common, followed by pulmonary hypertension (PH).[19] This heterogeneity in disease, coupled with the limitations of diagnostic tools and our understanding of the response to therapy makes it nearly impossible to predict the patient's health outcomes.[23] Therefore, a personalized approach that considers patient-specific data to assess the condition and make future predictions is recommended for the management of the condition.[23,24] One method that can transform the personalized care of patients with COPD is the use of mathematical models, which describe the respiratory system using standard engineering-based equations and parameter values estimated from individual patient data. Though several models of the human cardiovascular and respiratory systems have been proposed in the past, most of them are not designed to capture the physiology specific to COPD.[25−30] Hence, we recently proposed a model of COPD from a systems engineering perspective, whereby the

cardiorespiratory system was represented as a control system (sensor, controller, actuator, and process) and the disease state was modeled as a malfunction of one or more components of the system.[24,31] In the present work, we improve upon this model by including additional physiological phenomena, formalizing the model adaptations for the disease state and identifying optimal model parameters to analyze the patient dynamics under varying activity levels.

Our earlier analysis of COPD[24] was performed under the assumption of constant metabolic rates—that of the body at rest. This is a significant limitation, as those vary as a result of any significant physical activity. At increased activity levels, multiple modifications in the original model equations are required to appropriately describe the underlying physiology. For example, the cardiorespiratory control under high activity is primarily realized by a feedforward control loop that is less relevant while at rest.[32] The role of stomach muscles in active exhalation of air at high respiratory rates, the decreasing dynamic compliance of the lung and the increasing dead space at high tidal volume, and the multiple changes in cardiovascular physiology that result in an increased cardiac output are additional aspects of the system physiology that become increasingly relevant as the metabolic rate increases. As changes in the activity level of COPD patients are known to drive responses that are of clinical interest—some of which we lack a clear mechanistic understanding of—it becomes imperative to introduce these features into the mathematical model used in the analysis of COPD.[33,34]

In ref 24 we proposed multiple model adaptations to represent the different manifestations of COPD. Small airway disease was modeled as an increase in airway resistance, emphysema was represented as a combined change in unloaded lung volume and lung elastance, and PH was characterized as a modification of the pulmonary arterial resistance. The parameters for adaptation were chosen from our understanding of disease pathophysiology. In the present work, we formally justify the selection of the parameters to
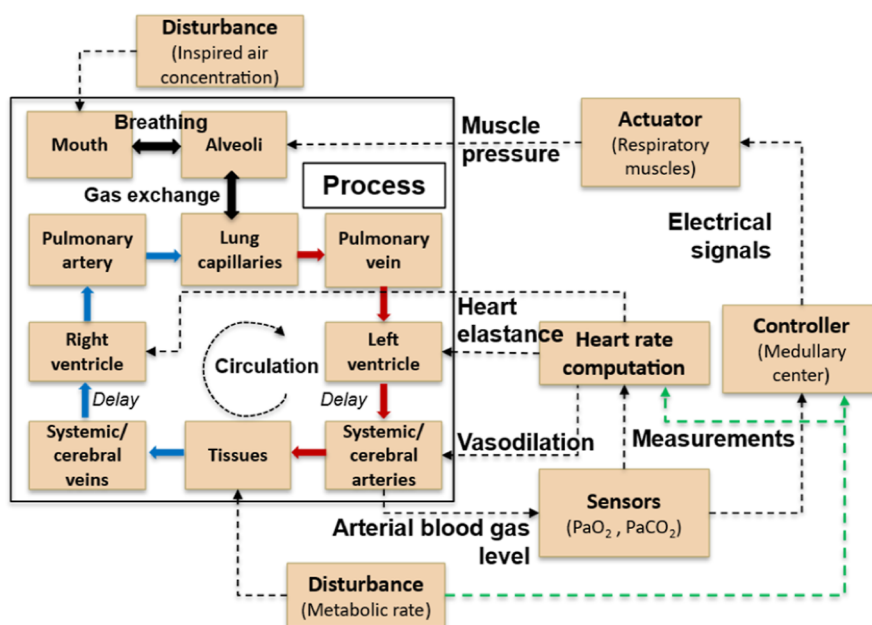
Figure 2. Block diagram representation of the cardiorespiratory system shown in Figure 1. The green lines indicate the feedforward loop introduced to the existing model in ref 24. Adapted with permission from ref 24. Copyright 2023, the authors.

adapt from our previous work with the help of sensitivity analysis.

Most of the model equations and parameters used in ref 24 were obtained directly from the literature. Though the response of the cardiovascular system was within acceptable limits of the clinically observed values, there were minor deviations, some of which could increase considerably as the activity level of the individual increases. Therefore, in the present work, we adaptively estimate a few selected parameters of the cardiovascular system to match clinically observed input−output data using a gradient-free optimizer called parallel tempering.[35] The algorithm uses a Monte Carlo-based stochastic approach to converge on a near-optimum parameter solution that is insensitive to the initial guess.

We arrange the rest of this article as follows: in Section 2, we describe the model enhancements and methodologies used in its analysis. In particular, the changes in the model involving the respiratory system are described in Section 2.1, those involving the cardiovascular system in Section 2.2, and the adaptation of parameters to represent COPD are discussed in Section 2.3. In the remaining two subsections of Section 2 (2.4 and 2.5), we present an outline of the formal sensitivity analysis and of the parallel tempering, which is the stochastic global optimization method used for parameter estimation. In Section 3, we present the analysis and simulation results, compare them with reports from past experiments, and provide a related discussion. This includes simulation results of the healthy state (3.1), and parameter adaptations and simulation results of the disease state (3.2). The key conclusions of the study are summarized in Section 4.

2. MODEL AND ANALYSIS METHODOLOGY

In earlier work, we presented a dynamical system model of the human cardiorespiratory system developed through integrating existing models of different subsystems.[24] The system comprised modules representing the physiological components and functions involved in the processes of breathing, gas exchange, blood circulation, and their control as shown

schematically in Figure 1a (see ref 24 and its Supporting Information for details on the physiology and a summary of the model). The approach followed standard process engineering and control-based modeling, as, for example, shown in Figure 1b, for controlling the cooling of an exothermic reactor. Mathematical equations (ordinary differential and algebraic) representative of each module were taken from the existing literature, and the parameter values were either directly obtained or were computed from the input−output data. The system comprising the process (cardiorespiratory system), sensors (chemoreceptors), controller (neural control), and actuators (chest and heart muscles) were simulated under normal and anoxemic conditions to verify the predictive capabilities of the model. The different manifestations of COPD were represented within the physiological model as parameter adaptations that were quantified based on changes in clinically relevant systemic responses. For example, small airway disease was represented by an increase in airway resistance. The parameter value was chosen such that the model response (spirometry test; see ref 24 and its Supporting Information) was similar to that observed in a patient with the condition. Though we did not explicitly perform a model order reduction, the model itself was a reduced one with all biological phenomena represented by simplified equations derived from experimentally observed relationships between biological variables. In this bottom-up approach, we produced an engineering model that has the minimum number of parameters and complexity rather than a pure first-principles-based approach.

In ref 24, the modeling and simulations were performed under the assumption that the metabolic rates remained constant (the physical exertion in different activities is quantified as the metabolic equivalent of tasks—R_m—based on the oxygen consumed, where $R_{m=1}$ at resting conditions[36]). In the present work, to understand the dynamics of cardiovascular and respiratory variables of COPD patients under varying metabolic rates, we extended the systems engineering model of the human cardiorespiratory system to
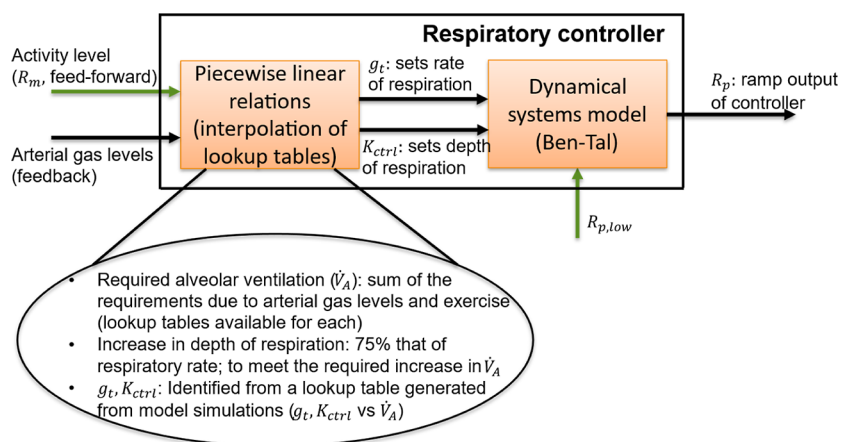
Figure 3. Schematic of the respiratory control model. The model now considers the activity level (R_m, highlighted by the green arrow) in addition to the arterial gas concentrations to give the electrical signal (R_p) to the lung/chest muscles. It also considers a more involved model of $R_{p,low}$.

include a few additional physiological processes: a feedforward loop in cardiorespiratory control, the role of stomach muscles in active exhalation, the varying compliance of the lung at high alveolar volumes, and the changes in cardiovascular parameters to increase the cardiac output. The modular structure of the process model allows us to efficiently implement these changes without affecting the remaining model equations. A description of the updates is provided below (Sections 2.1, 2.2, and 2.3) and the complete set of model equations and parameter values are available in the Supporting Information. It may be noted that a few modifications of the base model ($R_{m=1}$) were also required, as any errors there could amplify as the metabolic rates increased. These changes do not negate the qualitative insights given in the previous work, rather they improve it in a quantitative sense.

2.1. Changes in the Respiratory System and Control. During strenuous exercise, the ventilatory requirements of the human body increase due to the increased oxygen demands. As a response to this, we observe an increased respiratory rate and circulation of blood. One could potentially ascribe this regulation to the feedback control loop that modifies the heart and respiratory rates based on the gas concentrations in the blood, as described in ref 24. However, on observing the dynamics of the heart and respiratory variables in humans, their exercise response is almost instantaneous, much before there are any noticeable changes in the blood gas levels, revealing the existence of an almost perfect feedforward control loop triggered by the activity level of the individual. It is therefore believed that the brain, upon initiating the motor impulses for stimulating the muscles involved in the exercise, also sends collateral impulses to the brainstem to excite the cardiovascular and respiratory control centers, resulting in increased respiratory drive and cardiac output.[32] This feedforward loop appears to be dominant in the regulation of the cardiorespiratory systems during exercise, and the chemoreceptor-based feedback loop merely fine-tunes the variables over a much slower time scale. Hence, in the mathematical model, we introduced a feedforward control loop for the regulation of respiration and heart rate, as shown by the green dashed lines in the block representation of the cardiorespiratory system in Figure 2. The following subsections describe the implementation of this feedforward loop and a few other improvements in the model of the cardiorespiratory system proposed earlier in ref 24

2.1.1. Feedforward Loop for Respiratory Control. In our model, the respiratory control is primarily based on the model by Ben-Tal and Smith[37] which combines an oscillator with an inspiratory pattern generator (leaky integration) to regulate the depth and frequency of respiratory cycles (see Supporting Information of ref 24). The associated chemoreceptor-based feedback control system was designed to drive the controller output signal, R_p depending on the available measurements of arterial gases. Under varying activity levels, the feedback controller we used would not be activated on time due to the transport delay in circulation. This delay resulted in substantial deviations of blood gas levels, sometimes even instability of the system. This pointed to the necessity of an additional feedforward loop—the existence of which is well documented in textbooks on physiology[32]—in maintaining system stability. In the present work, we included the exercise-dependent feedforward loop as an additive term modifying the controller variables g_t (affecting the respiratory frequency) and K_{ctrl} (affecting the respiratory amplitude) as shown in Figure 3. It may be noted that the two control loops while being designed with the common goal of maintaining blood gas levels, worked toward rejecting disturbances from different sources. Hence, they were modeled as parallel loops rather than in cascade.

Existing data on the variations of alveolar ventilation as a function of activity levels and arterial gas concentrations were used to choose the values of the controller variables.[32,38] That is, for a given metabolic rate, the corresponding alveolar ventilation required was determined through linear interpolation of the data in a lookup table (Figure S5 in Supporting Information). This was then added to the contributions from the chemoreceptor-based feedback loop, which were also obtained through linear interpolation of the available data on blood gas levels and alveolar ventilation. Having identified the total alveolar ventilation required, the next task would be to choose the controller variables g_t and K_{ctrl} that would drive this ventilatory response. It is unclear to us how the brain partitions the increased requirements in alveolar ventilation between depth and frequency of breathing.[39] We, therefore, increased the frequency and depth of the breathing process in the ratio 4:3, which is the average increase reported in ref 38. For this, another table created from open-loop simulations of the controller model at different values of g_t and K_{ctrl} was used. The resultant controller was primarily of proportional type, with the proportional gain being a function of the system state. A

schematic showing this controller implementation is given in Figure 3, and the input−output data used in this model are provided in Figure S5. The fractional changes in ventilation were used rather than the absolute values to enable compatibility between data from multiple sources.

2.1.2. Role of the Stomach in Active Exhalation. The model of lung mechanics in refs 24 and 37 introduces the respiratory drive primarily through the contraction of the diaphragm which is modeled as a dynamical system. The exhalation is passive, brought about by the pressure existing in the lungs on the relaxation of the diaphragm. At higher activity levels, the respiratory rates increase, and the pressure in the lungs is no longer sufficient to complete the exhalation within the available time. Therefore, the muscles in the stomach provide the additional pressure required to exhale the air. Molkov et al.[40] represented this role of the stomach as a second dynamical system alongside the existing one for the diaphragm. In the present work, we introduce this effect as an additive term to the controller's ramp output R_p as this functional form was successfully used to simulate a deep breath (which involves the stomach muscles) in ref 24. $R_{p,low}$, the lower limit of R_p—which earlier equaled zero under all conditions—is now modeled as described in eq 1.

$$R_{p,low} = \begin{cases} 0, & rr_{-1} < 15 \\ R_{p,low,db}\dfrac{(rr_{-1} - 15)}{(37 - 15)}, & rr_{-1} \geq 15 \end{cases}$$

(1)

where $R_{p,low,db} = -2$ is the lower limit of R_p used in the simulation of the deep breath (see Section S2 of Supporting Information for details on spirometry), and rr_{-1} is the respiratory rate calculated from the previous breath. To ensure that respiration was completed within the available time, the response time of the lung muscles (the actuator) also had to be reduced. For this, the time constants of the dynamical system were updated as given in eq S37.

2.1.3. Dynamic Compliance of the Lung as a Function of Alveolar Volume. In ref 24, the compliance of the lung was assumed to remain constant with the alveolar volume, as this has been experimentally observed under normal conditions.[41] However, under strenuous exercise, tidal volumes increase substantially, and the dynamic compliance decreases as described in ref 42. Therefore, in the extended mathematical model, the lung compliance was retained for up to an alveolar volume of 5 L (V_{th}), above which the dynamic compliance is gradually reduced to zero—the resultant alveolar volume converging to 7 L (V_{max}). The static elastance (inverse of static compliance) is given by eq 2, and the alveolar volume as a function of transpulmonary pressure is shown in Figure 4. It may be noted that this modification does not affect lung volumes under normal breathing, as evident from Figure 4.

$$E_T = \begin{cases} E_{T0} & \dfrac{P_A}{E_{T0}} < V_{th} \\[3mm] \dfrac{P_A}{V_{max} - V_0 - (V_{max} - V_{th})e^{\left(\frac{V_{th} - V_0 - P_A/E_{T0}}{V_{max} - V_{thres}}\right)}} & \dfrac{P_A}{E_{T0}} \geq V_{th} \end{cases}$$

(2)

2.1.4. Lung Dead Space as a Function of Tidal Volume. The lung dead space refers to the volume of air in the lung that fills the bronchial tubes and does not actively participate in gas exchange. This quantity was assumed to be a constant in the
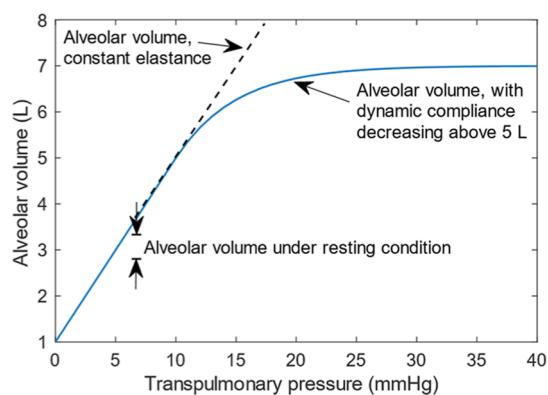
Figure 4. Alveolar volume as a function of transpulmonary pressure. At high pressures, the volume converges to a maximum of 7 L.

previous model.[24] However, at high respiratory rates, as the tidal volume increases, the dead space, V_D, also increases.[38,43] Therefore, following what was reported in ref 38, in the extended model, the dead space was made a linear function of the tidal volume (eq 3), varying between 0.15 L at rest (tidal volume, $V_{T,min} = 0.5$ L) and 0.3375 L at peak exercise (tidal volume, $V_{T,max} = 1.8$ L)

$$V_D = V_{D0}\left(1 + \frac{1.25(V_{T,-1} - V_{T,min})}{V_{T,max} - V_{T,min}}\right)$$

(3)

where $V_{T,-1}$ is the tidal volume recorded in the previous breath and V_{D0} is the tidal volume at rest ($=0.15$ L).

2.2. Changes in the Cardiovascular System and Its Control. *2.2.1. Feedforward Loop for Cardiovascular Control.* The cardiac output in the human body almost quadruples when an individual transitions from rest to peak activity levels. The increased circulation is a result of changes in heart rate, contractility, afterload, and preload.[44] To represent this in the mathematical model, the exercise-based feedforward loop was designed to increase the heart rate, H, linearly with the metabolic rate[45] from a baseline value of 60 to 180 bpm at peak exercise ($R_m = 10$). This was introduced as an additive term to the existing chemoreceptor-based feedback loop, which is now responsible for removing any remaining disturbances. The new term is given by H_M in eq 4 (see Supporting Information for a description of the terms appearing in the chemoreceptor-based contribution, H_{O_2,CO_2}).

$$H = H_M + H_{O_2,CO_2}$$

$$H_M = \frac{(R_m - 1)(180 - 60)}{9}$$

$$H_{O_2,CO_2} = \frac{1}{CBF_f {}^* H_c}(750 + W(h_1(P_{CO_2,Sa})^5 + i_1(P_{CO_2,Sa})^4 \\ + j_1(P_{CO_2,Sa})^3 + p_1(P_{CO_2,Sa})^2 + q_1 P_{CO_2,Sa} + r_1 \\ + f(g - P_{O_2,Sa})^s))$$

(4)

2.2.2. Changes in Other Cardiovascular Variables. A few additional cardiovascular parameters were updated to obtain systemic responses (cardiac output and arterial pressures) that better resemble standard values at rest and exercise. Based on the experimental data reported in refs 46 and 47, the arterial resistances (R_s, systemic; R_p, pulmonary) and the systemic compliance (C_{sa}) were set to reduce by 60% and 50% from

their original values, respectively, as the heart rate increased from 60 to 180. The remaining targeted parameters were determined through a sensitivity analysis, such as pulmonary arterial compliance (C_{pa}), heart valve resistance ($R_{v,o}$), left ventricular elastance (systolic, $E_{s,l}$), and right ventricular elastance (diastolic, $E_{d,r}$). The optimal values for these chosen parameters were identified by solving an estimation problem using the parallel tempering algorithm, described later in Section 2.5. This simulation-based optimization problem had the objective of minimizing the deviation of the predicted systolic and diastolic pressures, mean pulmonary arterial pressures, and cardiac output from their respective standard values, as given in eq 5. At a heart rate of 60 beats/min, the targets were systolic and diastolic pressures of 120/80 mmHg, cardiac output of 80 mL/s, and mean pulmonary arterial pressure of 17 mmHg.[32,48] At a heart rate of 180 beats/min (higher activity level), the targets were systemic arterial pressures of 180/80 mmHg, cardiac output of 360 mL/s, and mean pulmonary arterial pressure of 25 mmHg.[38,48] The squared deviations were scaled using the respective standard values to give weights similar to those of all terms in the objective function. Though this step also modified some of the parameter values at rest, the changes were minor causing little or no qualitative changes in the results reported earlier in ref 24.

$$\min_{\substack{\theta=\{R_{v,o}, \\ C_{pa(H=60)},\, C_{pa(H=180)}, \\ E_{d,r(H=60)},\, E_{d,r(H=180)}, \\ E_{s,l(H=60)},\, E_{s,l(H=180)}\}}} \sum_i \left(\frac{y_{i,\text{pred}} - y_{i,\text{target}}}{y_{i,\text{target}}} \right)^2$$
$$\text{s.t. } \mathbf{y}_{\text{pred}} = F_c(H, \theta) \tag{5}$$

where $y_{i,\text{pred}}$ are the model responses (systemic arterial pressures; mean pulmonary arterial pressure $\langle P_{pa} \rangle$, and cardiac output q_{sa}) that we desire to make equal to their respective clinically observed values ($y_{i,\text{target}}$), and F_c denotes the mathematical model of the cardiovascular system.

The updates made in the respiratory and cardiovascular systems are summarized in Table 1.

Table 1. Summary of Model Updates

component	update	references
control of heart and respiratory rates	included a feedforward loop based on metabolic rates	32 and 38
respiratory muscles	included the role of the stomach in active exhalation at high activity levels	40
lung compliance	reduced dynamic compliance of the lung at high alveolar volume	42
lung dead space	lung dead space increases with tidal volume	38 and 43
cardiovascular parameters	adjusted to be better representative of system dynamics at low and high activity levels	32,38, and 46−48

2.3. Model Adaptations in COPD. To adapt the model for COPD, a few parameters with the largest effect on COPD manifestations viz. small airway disease, emphysema, and PH were chosen through a sensitivity analysis. The specific parameter perturbations that resulted in COPD-like responses were identified by solving simulation-based optimization problems using the parallel tempering algorithm described later in Section 2.5. The cost function for these estimation problems (eq 6) used target values of FEV1 ratio (0.7; the ratio of air expired out in 1 s to that of the total air expired out in a spirometry test), total lung capacity (6.6 L; TLC), functional residual capacity (4 L; FRC), and mean pulmonary arterial pressure (35 mmHg) to guide the optimization.[19,49,50] These values were selected based on their use in diagnosing COPD. The airway resistance was the decision variable to meet the targeted FEV1 ratio; the chest elastance and unloaded lung volume were perturbed to meet the TLC and FRC targets, and the pulmonary resistance was adjusted to meet the targeted pulmonary arterial pressures. The objective function was the squared deviation of the model response from the targets.

$$\min_\theta \sum_i \left(\frac{y_{i,\text{pred}} - y_{i,\text{target}}}{y_{i,\text{target}}} \right)^2$$
$$\text{s.t. } y_{\text{pred}} = F_r(\theta) \tag{6}$$

where y_i are the systemic responses and F_r denotes the mathematical model of the respiratory system. The subscripts *pred* indicate model predictions and *target* indicate the standard values observed in COPD patients. The decision variables (θ), the systemic responses, and their target values in different COPD manifestations are given in Table 2.

Table 2. Decision Variables, Model Responses, and Their Target Values in Different COPD Manifestations

manifestation	θ	systemic response (y_i)	target value ($y_{i,\text{target}}$)
small airways	airway resistance (R)	FEV1 ratio	0.7
emphysema	lung elastance (E_T), unloaded lung volume (V_0)	TLC, FRC	6.6 L; 4.0 L
pulmonary hypertension	pulmonary arterial resistance (R_{pa})	mean pulmonary arterial pressure ($\langle P_{pa} \rangle$)	35 mmHg

Previously, in ref 24 the parameters were chosen based on our understanding of the disease pathophysiology. The present work uses a more systematic approach, first with the sensitivity analysis,[51,52] then using a parallel tempering algorithm, a multiparameter optimization tool that is known to be efficient in solving parameter estimation problems involving dynamical systems.[35]

2.4. Sensitivity Analysis. To understand the relative contribution of each cardiorespiratory parameter to the overall systemic behavior and disease states related to COPD, we performed a global sensitivity analysis. Here, the objective was to identify parameters to which the systemic responses (cardiorespiratory variables of clinical significance) were sensitive.

A density-based global sensitivity analysis approach known as PAWN[53] was selected because the underlying distribution of the outputs of interest was unknown and because it has been used to analyze the parametric sensitivity of other cardiovascular system models.[54,55] To determine the underlying distribution, PAWN utilizes cumulative density functions (CDFs) to characterize model outputs of interest one at a time. The first set of simulations varies all parameter inputs simultaneously to produce unconditional CDFs. A second set of simulations varies all inputs except for the parameter of interest to produce conditional CDFs. To determine the

parametric sensitivity index for the i-th input factor, the Kolmogorov−Smirnoff (KS) statistic (S) is used to quantify the distance between the unconditional and conditional CDFs (F), as given by eq 7.

$$S_i = \underset{x_i \ y}{\mathrm{statmax}} |F_y(y) - F_{y|x_i}(y|x_i)| \tag{7}$$

Because the KS statistic depends on the value of the constant parameter, the PAWN method calculates the KS statistic for multiple values. We combine these statistics using a summary statistic (e.g., median) to characterize the distribution of the KS statistic. This summary statistic (PAWN index) varies from 0 to 1, with a value closer to 1 indicating a greater parametric influence on the output. To determine a threshold value for significant PAWN indices, the PAWN method introduces a dummy parameter that has no effect on the output. If the PAWN index of a parameter is greater than this value, then it is likely that the output is sensitive to that input parameter.

In the analyses reported here, the parameters were varied over a $[x/1.25, x \times 1.25]$ range from the nominal value. We performed 2000 simulations with six conditioning intervals and checked for convergence. The PAWN method also includes bootstrapping to determine 95% confidence intervals for each sensitivity index. Sensitivity indices were determined separately for the cardiovascular and respiratory systems. Each system was isolated from the rest of the model for all sensitivity analysis simulations because it was assumed that cardiovascular system parameters have a limited effect on respiratory function and vice versa. Respiratory system outputs were measured during a simulated deep breath once the system reached a time-periodic stationary state (TPSS) after a 38 s period. Cardiovascular system outputs were measured as the average over a 60 s period, once the system reached TPSS after a 30 s equilibration period.

2.5. Optimization Routine—Parallel Tempering. To solve the mathematical problems for identifying optimal parameter values, we used a gradient-free optimizer. We chose to use the stochastic annealing-based optimizer called parallel tempering due to its robust design and insensitivity to the initial guess.[35] The algorithm is an improvement to the well-known simulated annealing[56] based on a scientific formulation as described in ref 57. Parallel Tempering has proven convergence to the optimum if one waits long enough. From an engineering perspective, we waited until the changes in the objective function were below a certain threshold. The use of different initial guesses showed that the sensitivity and the final solution were not sensitive to the initial guesses.

The algorithm directs a biased random walk through the parameter space to converge toward a minimum value of the cost function. At each instance of the random walk, a new cost function is computed with a new set of parameters. The new parameters are accepted based on the Metropolis acceptance probability[35,58] (eq 8)

$$P_{\text{accept}} = \begin{cases} 1, & F_{\text{cost,new}} \leq F_{\text{cost,old}} \\ \exp\left(-\dfrac{F_{\text{cost,new}} - F_{\text{cost,old}}}{E_B}\right), & F_{\text{cost,new}} > F_{\text{cost,old}} \end{cases} \tag{8}$$

where P_{accept} is the probability that the new set of parameters will be accepted, $F_{\text{cost,new}}$ is the cost function value for the new set of parameters, $F_{\text{cost,old}}$ is the cost function value for the old

set of parameters, and E_B is the Boltzmann energy level. This probability equation allows a chance for the new parameter set to be accepted, despite producing a worse cost function value. The probability of accepting a worse parameter set scales with the Boltzmann energy. At lower E_B, the chance of making a random move toward a higher cost function value is minimal. At higher E_B values, random jumps to higher cost function values are more likely, which allows the algorithm to escape local minima. In the standard simulated annealing, there is an annealing schedule, which determines how fast the system moves from high temperature (high E_B) to low (low E_B), and the final parameter set can be highly dependent on the annealing schedule.[59] In parallel tempering, the annealing schedule is removed. Parallel tempering takes advantage of the benefits from both high and low Boltzmann energies and uses parallel runs, each with different constant Boltzmann energy levels. Occasionally these parallel runs exchange information with their closest Boltzmann level so that good cost function values are held at the low energies and new minima are found at the high energies. A schematic of the parallel tempering procedure is shown in Figure 5. This method allows the optimization to search the space both broadly in the hot sections and conservatively in the cold sections. The cost function evaluations are done with parallel processing to improve computational efficiency and the method for implementing the parallel tempering algorithm from ref 35 is followed.
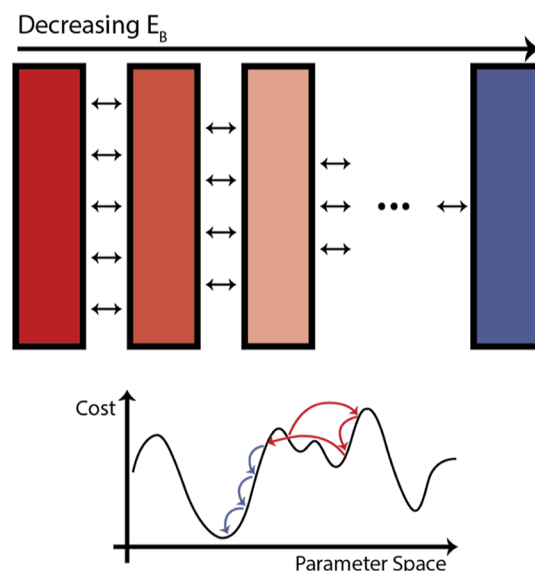
Figure 5. Schematic representation of the parallel tempering algorithm. Stochastic Monte Carlo routines are run in parallel at different constant Boltzmann energy levels. The hotter (red) runs are more likely to accept parameters with a poorer cost function value to exit the local minimum as shown. The colder (blue) runs are more likely to slowly proceed to the nearest minimum, as shown in the graph.

3. RESULTS AND DISCUSSION

3.1. Results for Healthy Individuals. Here, we report the results obtained from an analysis and simulations involving the model of the cardiorespiratory systems applied to healthy individuals. All simulations were performed by using MATLAB/Simulink R2020b.
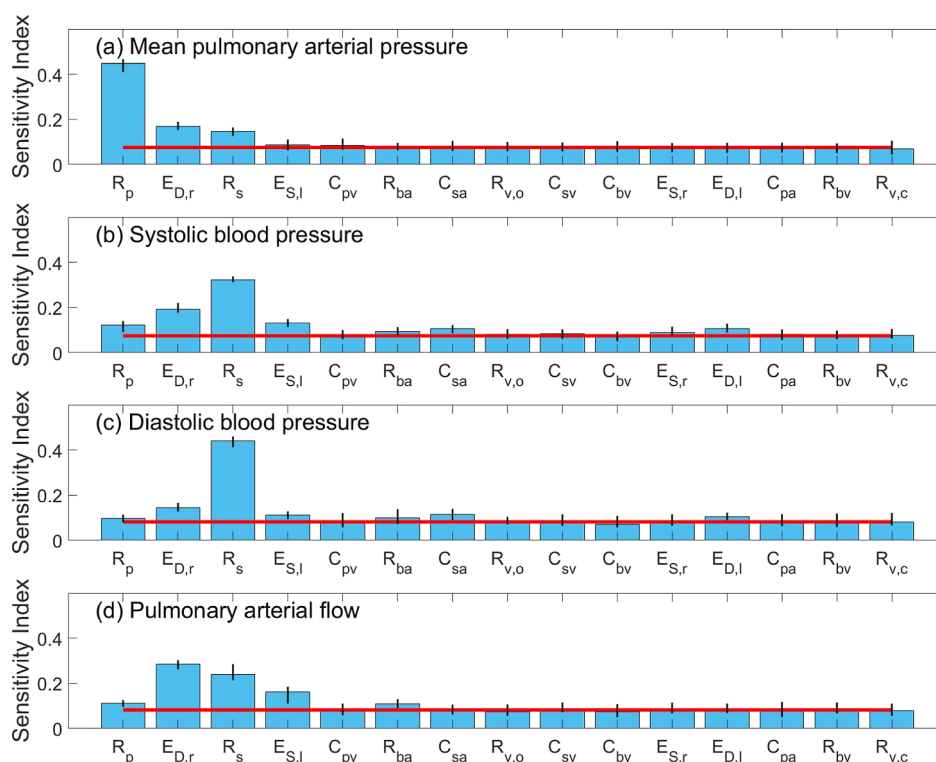
Figure 6. Global sensitivity analysis of cardiovascular parameters: mean pulmonary arterial pressure (a), systolic blood pressure (b), diastolic blood pressure (c), and pulmonary arterial flow (d). Sensitivity index varies from zero to one. Values closer to one have a larger effect on the output of interest. Parameters with a sensitivity index above the red line are significant. C_{pv}, pulmonary venous compliance; R_p, pulmonary resistance; $R_{v,o}$, heart valve resistance, open; $R_{v,c}$, heart value resistance, closed; $E_{d,l}$, left ventricular elastance, diastolic; $E_{s,l}$, left ventricular elastance, systolic; $E_{d,r}$, right ventricular elastance, diastolic; $E_{s,r}$, right ventricular elastance, systolic; C_{sa}, systemic arteries compliance; R_s, systemic arteries resistance; C_{sv}, systemic venous compliance; C_{pa}, pulmonary artery compliance; R_{ba}, brain arteries resistance; R_{bv}, brain veins resistance; and C_{bv}, brain veins compliance.

3.1.1. Sensitivity Analysis of the Cardiovascular System. Parameters to estimate for tuning the cardiovascular system were selected by using a global sensitivity analysis. The response variables—mean pulmonary arterial pressure, systolic pressure, diastolic pressure, and pulmonary arteries flow rate—were selected for their clinical significance (Figure 6). The parameters pulmonary resistance, right ventricular elastance (diastolic), systemic arterial resistance, left ventricular elastance (systolic), left ventricular elastance (diastolic), systemic arterial compliance, and brain artery resistance were found to have a significant effect on at least one of the cardiovascular response variables of interest. Systemic arterial resistance and right ventricular elastance (diastolic) were the only two parameters that affected all four response variables significantly. Pulmonary resistance was the most significant parameter affecting mean arterial pressure and did not significantly affect the other cardiovascular response variables.

3.1.2. Critical Parameter Estimation of the Cardiovascular System. The optimal values of the critical cardiovascular parameters identified by the sensitivity analysis were found by solving the mathematical problem described in Section 2.2.2. The optimal parameter values are listed in Table 3. The corresponding cardiac output and arterial pressures at the optimal parameter values are shown in Figure 7. On increasing the heart rate from 60 to 180, the cardiac output—indicated by the flow rate in the pulmonary arteries—increased from 86 to 320 mL/s. Systolic pressure increased linearly from 115 to 186 mmHg, a trend consistent with experimental observations.[60] This baseline systolic blood pressure at a heart rate (60–70

bpm) is consistent with other cardiovascular models[54,55] and is within one standard deviation of the average systolic blood pressure (123 ± 11) measured in healthy women.[61] In comparison, the diastolic and mean pulmonary arterial pressures had only a minor increase, as observed clinically (Table 3).

Table 3. Optimal Parameter Values of the Cardiovascular System

| parameter name	parameter symbol and unit	existing value	optimal values, HR = 60	optimal values, HR = 180
systemic arterial resistance	R_s [mmHg s/mL]	1.08	1.24	0.52
pulmonary arterial resistance	R_p [mmHg s/mL]	0.198	0.145	0.060
systemic arterial compliance	C_{sa} [mL/mmHg]	2.4	1.2	0.6
pulmonary arterial compliance	C_{pa} [mL/mmHg]	4.52	4.52	3.62
resistance at valves (open)	$R_{v,o}$ [mmHg s/mL]	0.0010	0.0017	0.0017
right ventricular elastance (diastolic)	$E_{d,r}$ [mmHg/mL]	0.0667	0.0786	0.0336
left ventricular elastance (systolic)	$E_{s,l}$ [mmHg/mL]	0.849	1.698	2.851
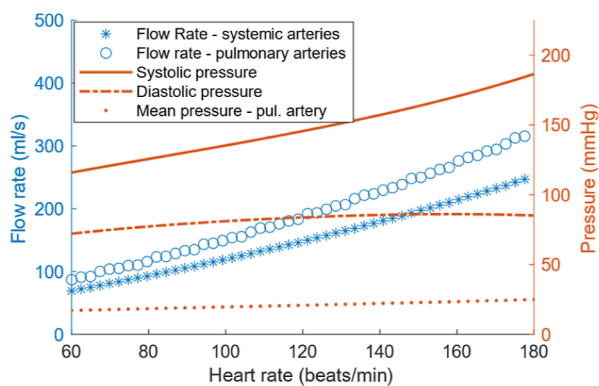
Figure 7. Arterial flow rates and pressures predicted by the model at varying heart rates.

3.1.3. Model Verification—Effect of Exercise on Blood Gas Levels. To verify the predictive capabilities of the model, we replicated a case reported in the literature by Holmgren and Linderholm.[62] Here, the authors recorded the heart rates and blood gas levels of a few healthy individuals under varying levels of activity. To replicate this, the model was simulated under five different metabolic rates, varying from the rest to peak exercise. The first 1000 s of the model simulations were discarded to allow the model to reach TPSS. After this, the model was simulated for 700 s under each activity level, of which the last 200 s was chosen for reporting (the remaining time was for the model to reach TPSS). Figure 8 shows the heart rate and minute ventilation values predicted by the mathematical model. The heart rates measured by Holmgren and Linderholm[62] are also added for comparison. Figure 9 shows the partial pressures of oxygen and carbon dioxide in the systemic arteries predicted by the model and those recorded by Holmgren and Linderholm[62] in their experiments. The predictions are in good agreement with the decreasing oxygen and carbon dioxide tensions measured in the experiments. The decrease in oxygen levels stimulated increased ventilation and perfusion, which in turn improved the exchange of carbon dioxide, resulting in lowered carbon dioxide tension. It may be noted that while the heart and respiratory rates were trained on data similar to those in ref 62, the blood gas levels were predictions made by the model with no related training data.

*3.1.4. Model Verification—Effect of Exercise on the Expiratory Flow-Volume Loops.* Respiratory flow-volume
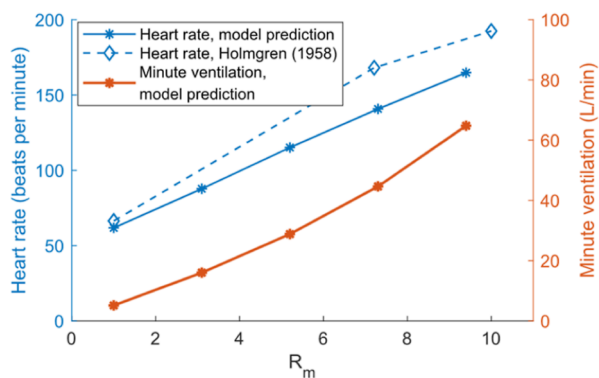
Figure 8. TPSS values of heart rate and minute ventilation at different activity levels (R_m). Reference data obtained with permission from Holmgren and Linderholm.[62] Copyright 2008, John Wiley and Sons.
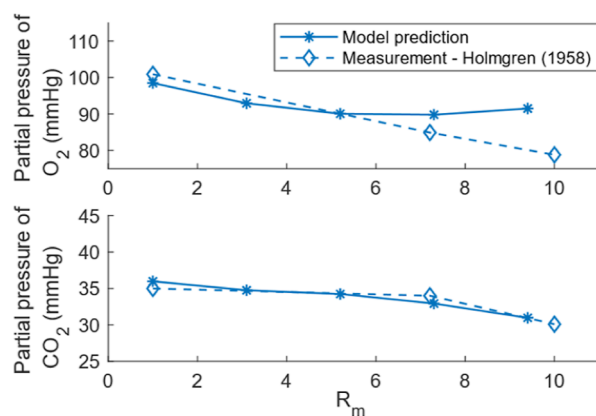

Figure 9. Arterial gas tensions in healthy individuals at different activity levels compared with the measurements made by Holmgren and Linderholm.[62] Reference data obtained with permission from Holmgren and Linderholm.[62] Copyright 2008, John Wiley and Sons.

loops are commonly used in the analysis of respiratory health. These plots report the expiratory air flow rates (*y*-axis) against the volume of gas expired (*x*-axis). In Figure 10, we plot the expiratory flow-volume loops at all activity levels considered in Section 3.1.3 and during a spirometry test (see Section S2 for a description of the test). As the metabolic rate increased from rest to that of peak activity level, the tidal volume increased from 0.45 to 1.83 L. The expiratory reserve volume (ERV; indicated by the right end of the flow-volume loops) and the FRC (the sum of the ERV and unloaded lung volume) decreased as the metabolic rates increased. The fractional drop in FRC (26%) was comparable to the drop recorded in measurements by ref 63 (~20%). The spirometry plot showed a peak expiratory flow rate (PEFR) of ~7 L/s and an FEV1 ratio of 0.88.
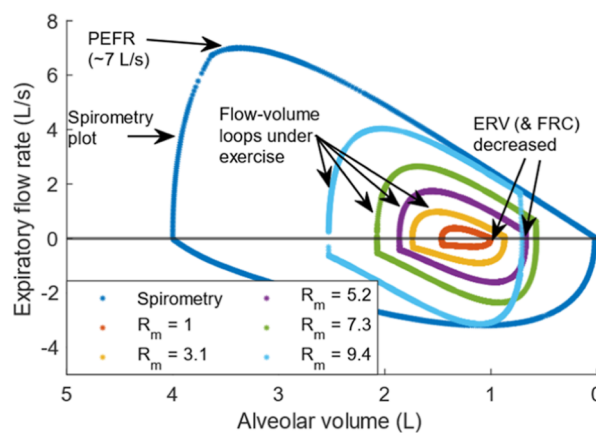

Figure 10. Expiratory flow-volume loops at different activity levels (R_m). Here, the *y*-axis shows the flow rate of expired air and the *x*-axis shows the volume of air left in the lung. The outermost loop shows the flow rates during a spirometry test.

3.2. Results for COPD Patients. *3.2.1. Sensitivity Results of the Respiratory System and Parameter Adaptation for COPD.* In the next step, the model parameters were adapted to represent the COPD patients. A similar step was performed in refs 19 and 63. However, the parameters were chosen based on knowledge of human anatomy and disease pathophysiology. Here, we report the results of a systematic global sensitivity
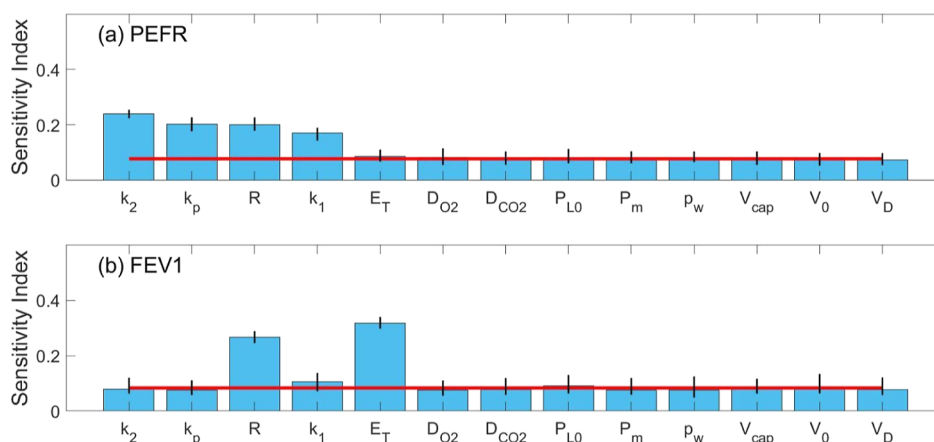
Figure 11. Global sensitivity analysis for model outputs used in clinical diagnosis of small airway disease. V_D, dead volume of lungs; R, airway resistance; p_w, vapor pressure, water; D_{O_2}, diffusion capacity, O_2; D_{CO_2}, diffusion capacity, CO_2; V_{cap}, capillaries volume; E_t, lung elastance; V_0, unloaded volume of lung; P_m, mouth pressure; P_{L0}, difference between atmospheric and pleural pressure; k_1, recoil constant of muscle; k_2, constant in equation of muscle; k_p, constant in equation of pleural pressure.
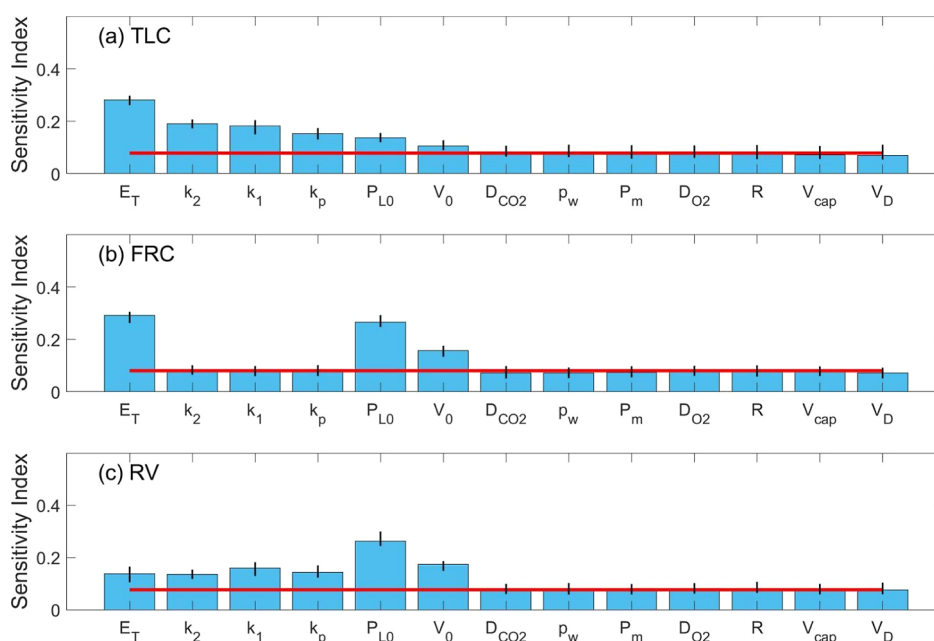
Figure 12. Global sensitivity analysis for model outputs used in the clinical diagnosis of emphysema. See Figure 8 for the variable names and abbreviations.

analysis for choosing the parameters and optimal parametric adaptations resulting in COPD-like responses.

3.2.1.1. Small Airway Disease. Small airway disease is a cardinal manifestation of COPD in which the thickening of airways leads to an increased resistance to the flow of air. The model responses representative of small airways are the PEFR and the FEV1 ratio.[19,64] The PAWN global sensitivity analysis was used to identify the selection of parameters for which the responses were sensitive (Figure 11). The relative contributions of respiratory parameters to the clinically diagnostic measurements of PEFR and FEV1 were evaluated. Lung elastance (Et) and airway resistance (R) contribute significantly to the changes in FEV1. The muscle constant (k_2), pleural pressure constant (k_p), airway resistance, and recoil constant (k_1) contributed significantly to PEFR. Airway resistance was the only common parameter that both outputs were sensitive to, supporting its selection as a parameter

representative of physiological changes occurring in small airway disease. The physiological manifestation of small airway disease as a decrease in airway size that restricts airflow reinforces the selection of airway resistance as a parameter representing the disease state. The optimal parameter adaptation for small airway disease was the one that resulted in an FEV1 ratio of 0.7,[64] realized at $\alpha = 0.27$.
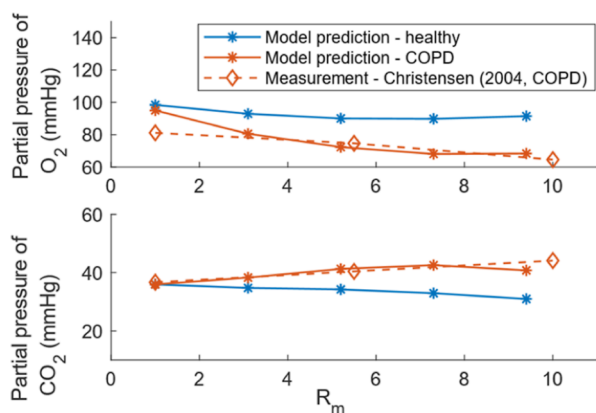
3.2.1.2. Emphysema. Emphysema is a COPD manifestation caused by damage to the alveolar walls, resulting in air entrapment and breathlessness. The agglomeration of alveoli and changes in lung elastance result in increased lung volumes. To model the adaptations for emphysema, a sensitivity analysis was performed to identify a selection of parameters that the lung volumes were sensitive to (Figure 12). The relative contributions of respiratory parameters to the clinically relevant respiratory metrics, TLC, FRC, and ERV were assessed. The common parameters that significantly affected

all three metrics were lung elastance (E_t), unloaded lung volume (V_0), and the atmospheric and pleural pressure difference (P_{l0}). Based on this analysis, lung elastance and unloaded lung volume were selected for tuning to represent COPD adaptations for emphysema. The selection of these parameters is reinforced by the decreased elastic recoil seen in the lungs of emphysema patients.[65] The difference between atmospheric and pleural pressure was not selected because it is more constrained physiologically and any effect it has is merely an addition to that of V_0 as evident from eqs S4 and S38. The optimal parameter values that were symptomatic of COPD were E_t = 1.9 mmHg/L and an unloaded V_0 = 1.63 L to meet the response variables (FRC and TLC) reported in ref 50.
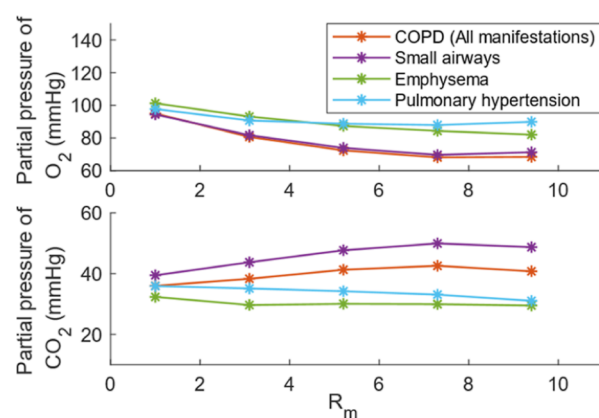
3.2.1.3. Pulmonary Hypertension. PH is a common condition in COPD in which the mean pressure of the pulmonary artery rises because of modifications in lung capillaries, causing stress on the right side of the heart. The global sensitivity analysis was repeated to identify the parameters resulting in increased pulmonary arterial pressure (Figure 6a). Pulmonary resistance (R_p) was found to have the highest effect on the response variable—mean pulmonary arterial pressure. The optimal parameter value of 0.422 mmHg.s/mL resulted in the targeted mean pulmonary arterial pressure ($\langle P_{pa} \rangle$) of 35 mmHg.[65]

With the parameter adaptations to represent different COPD manifestations, the model was used in simulations at varying levels of exercise. The results are described in the following subsections.

3.2.2. Effect of Exercise on Blood Gas Levels. The models (with different COPD adaptations) were simulated under varying activity levels for the same duration as those used for the healthy individuals presented in Section 3.1.3. The corresponding model predictions and measured literature for the arterial gas concentrations at the TPSS are given in Figure 13. In the experimental observations reported in ref 66, the arterial oxygen levels were lower and the carbon dioxide levels were higher in COPD patients as compared with those of healthy individuals. These results are reproduced well by our model. On comparing the different manifestations individually (Figure 14), all manifestations result in lower oxygen levels. However, the CO_2 levels remain close to normal in PH and emphysema potentially due to the increased respiratory rates.

Figure 14. Arterial gas concentrations in the COPD model when adaptations of different COPD manifestations are considered individually. Reference data obtained with permission from Christensen et al.,[66] Copyright 2004, Elsevier Science and Technology Journals.

3.2.3. Effect of Exercise on the Expiratory Flow-Volume Loops—Dynamic Hyperinflation. Figure 15 shows the expiratory flow-volume loops of the COPD patients. A drop in PEFR and an inward curvature at the terminal part of the spirometry plot (where the expiratory flow rate decreases from PEFR to zero) are observed, as expected in COPD.[64,67] In comparison with healthy individuals (Figure 10), the FRC does not decrease as much with an increase in activity levels. In fact, at high activity levels (R_m = 9.4), the FRC is larger than that at rest—a phenomenon commonly observed in COPD patients and referred to as dynamic hyperinflation (DH).[34,68,69] The plot of alveolar volumes at rest and peak activity levels (Figure 16) shows the DH more clearly on the volume—time axis. The effect of individual COPD manifestations on expiratory flow rates is shown in Figure 17 (PH was not considered as that was a cardiovascular change with a limited effect on respiratory mechanics). It is observed that small airway disease contributes more to DH than emphysema because, at higher activity levels, it is the airflow resistance that primarily prevents the lung from returning to its equilibrium position. It may be noted that these are not the features on which the model is explicitly trained, but rather are a result of the model adaptations for COPD described in Section 2.3.
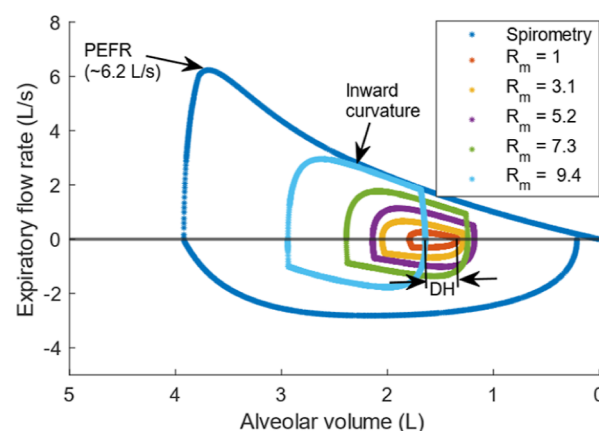

Figure 13. O_2 and CO_2 tensions in the systemic arteries of the COPD model (adaptations for all manifestations considered simultaneously). Reference data obtained with permission from Christensen et al.,[66] Copyright 2004, Elsevier Science and Technology Journals.

**Figure 15.** Expiratory flow volume loop in COPD patients when all parameter adaptations are included.
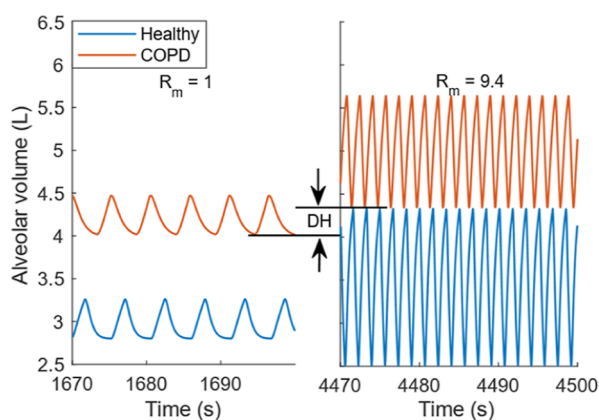
Figure 16. Plot of the variations in alveolar volume (healthy and COPD) under rest ($R_m = 1$) and peak exercise ($R_m = 9.4$). DH is shown by the shift in the equilibrium lung position.
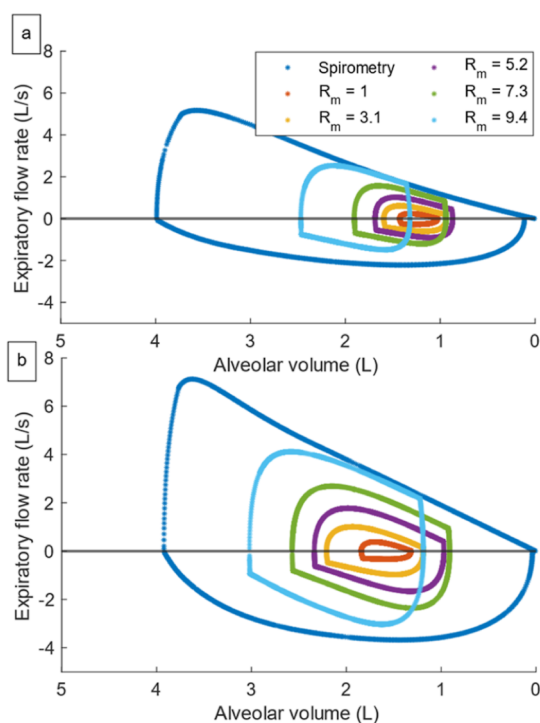
Figure 17. Expiratory flow-volume loops in (a) small airways and (b) emphysema.

3.2.4. Prospects for Remote Patient Monitoring. In Figure 18, we plot the heart and respiratory rates of healthy individuals and COPD patients at rest and moderately high activity levels. It is observed that the differences between the responses of the models are more pronounced at higher activity levels, indicating that these variables, in conjunction with the activity levels, contain information about the state of the disease. One could come up with an inverse relationship that determines the state of the patient from these measurements, which can easily be obtained from a wearable device. The results reinforce the possibility of completely automated remote patient monitoring (RPM) of COPD patients, as COPD exacerbations are expected to make these deviations even more pronounced. However, the hypothesis needs to be confirmed using personalized models and real patient monitoring data.
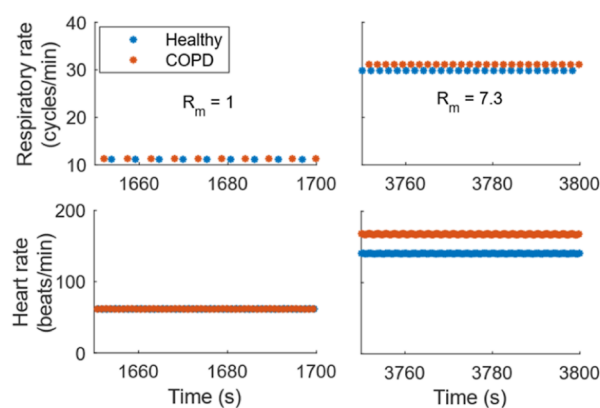
Figure 18. Heart and respiratory rates in healthy individuals and COPD patients (including adaptations for all manifestations) under rest and high activity levels.

3.3. Model Limitations. While the model we proposed here can replicate and predict several clinically relevant aspects of COPD, there are avenues for improvements. One part of the model that could benefit from additional details is the neural controller. At present, the respiratory controller is represented using an oscillator followed by a pattern generator.[40] The models used in refs 51, 54, and 69 for respiratory and cardiovascular control include finer details of the structure of the control system. The advantage of including such details is that it could allow for modeling neural adaptations in COPD patients. It is natural that stress caused by a decline in lung function would lead to adaptations in the control system. Analyzing the effect of such adaptations on the disease prognosis and the patients' quality of life could pave new paths for managing the condition—an aspect that we have not considered in this work.

The other important feature that is missing is the personalization of the model for individual patients. Given sufficient patient data, one could estimate the critical parameters identified in Sections 3.1.1 and 3.2.1 from the data rather than the population averages used in the present work.[51,70] This identification step may require improving computational performance using simpler models. In this context, it is worth exploring the development of hybrid modeling approaches—that combine data-driven and first-principles-based models—that are simple enough for parameter estimation while capturing the essential physics involved.[71−73]

4. CONCLUSIONS

In this work, we extended a previously developed control engineering model of the human cardiorespiratory system for healthy individuals and adapted it for COPD to accommodate variations in metabolic rates at different exercise levels. Several model improvements have also been implemented to accommodate the large variations in clinically important response variables observed at different levels of exercise. A sensitivity analysis was used to justify the selection of a set of critical parameters, the variations of which would fit the model predictions to experimental findings in healthy and disease states. Moreover, the optimal parameter values were determined using an in-house-developed stochastic global optimization algorithm.

The arterial gas levels of COPD patients predicted by the model at different activity levels were in good agreement with

the experimental observations reported in the literature. The model effectively replicated the shift in equilibrium lung positions observed in COPD patients (DH) and could distinguish between the disease manifestations that made patients more susceptible to DH, which, to the best of our knowledge, is the first instance of a dynamical system model capturing the physiology in DH. Furthermore, the simulation results reinforced the prospects of RPM in COPD patients—an aspect that has been attempted by multiple researchers in the recent past, but rarely in the light of the underlying physics.[33,74,75] In addition to aiding the development of RPM strategies, we believe the model will help elucidate the principles of gas exchange in COPD patients, particularly in DH, thereby guiding the selection of optimal intervention strategies such as noninvasive ventilation.[76]

◼ ASSOCIATED CONTENT

ⓈⒾ Supporting Information

The Supporting Information is available free of charge at https://pubs.acs.org/doi/10.1021/acsomega.3c05953.

> The Simulink file used in this work may be obtained from the corresponding author on reasonable request. The following additional works are referred to in the Supporting Information[77−90]
>
> Model equations, parameters, and the method for simulating the spirometry test (PDF)

◼ AUTHOR INFORMATION

Corresponding Author

Antony N. Beris − Department of Chemical and Biomolecular Engineering, University of Delaware, Newark, Delaware 19716, United States; ⓞ orcid.org/0000-0001-6033-0800; Email: beris@udel.edu

Authors

Varghese Kurian − Department of Chemical and Biomolecular Engineering, University of Delaware, Newark, Delaware 19716, United States

Michelle Gee − Department of Chemical and Biomolecular Engineering, University of Delaware, Newark, Delaware 19716, United States; Daniel Baugh Institute of Functional Genomics/Computational Biology, Department of Pathology and Genomic Medicine, Thomas Jefferson University, Philadelphia, Pennsylvania 19107, United States

Sean Farrington − Department of Chemical and Biomolecular Engineering, University of Delaware, Newark, Delaware 19716, United States

Entao Yang − American Air Liquide Inc., Newark, Delaware 19702, United States; ⓞ orcid.org/0000-0002-0420-8920

Alphonse Okossi − American Air Liquide Inc., Newark, Delaware 19702, United States

Lucy Chen − American Air Liquide Inc., Newark, Delaware 19702, United States

Complete contact information is available at:
https://pubs.acs.org/10.1021/acsomega.3c05953

Notes

The authors declare no competing financial interest.

◼ ACKNOWLEDGMENTS

◼ REFERENCES

(1) Stephanopoulos, G.; Reklaitis, G. V. Process systems engineering: From Solvay to modern bio- and nanotechnology. *Chem. Eng. Sci.* **2011**, *66* (19), 4272−4306.

(2) Stokes, C. L. Biological Systems Modeling: Powerful Discipline for Biomedical E-R&D. *AIChE J.* **2000**, *46* (3), 430−433.

(3) Kopach-Konrad, R.; Lawley, M.; Criswell, M.; Hasan, I.; Chakraborty, S.; Pekny, J.; Doebbeling, B. N. Applying Systems Engineering Principles in Improving Health Care Delivery. *Int. J. Gen. Med.* **2007**, *22*, 431−437.

(4) Bogle, I. D. L.; Allen, R.; Sumner, T. The Role of Computer Aided Process Engineering in Physiology and Clinical Medicine. *Comput. Chem. Eng.* **2010**, *34* (5), 763−769.

(5) Islam, M. A.; Cook, C. V.; Smith, B. J.; Ford Versypt, A. N. Mathematical Modeling of the Gut-Bone Axis and Implications of Butyrate Treatment on Osteoimmunology. *Ind. Eng. Chem. Res.* **2021**, *60* (49), 17814−17825.

(6) Navarathna, P.; Cameron, F.; Sontakke, M.; Yang, S.; Diamond, T.; Bequette, B. W. Machine-Learning-Based Detection of Pressure-Induced Faults in Continuous Glucose Monitors. *Ind. Eng. Chem. Res.* **2023**, *62* (5), 2255−2262.

(7) Harrold, J. M.; Parker, R. S. Clinically Relevant Cancer Chemotherapy Dose Scheduling via Mixed-Integer Optimization. *Comput. Chem. Eng.* **2009**, *33* (12), 2042−2054.

(8) Ragothaman, S.; Narasimhan, S.; Basavaraj, M. G.; Dewar, R. Unsupervised Segmentation of Cervical Cell Images Using Gaussian Mixture Model. *Proceedings of the IEEE Conference on Computer Vision and Pattern Recognition Workshops*, 2016.

(9) Sankar E M, A.; Rengaswamy, R. Droplet Microfluidic Networks as Hybrid Dynamical Systems: Inlet Spacing Optimization for Sorting of Drops. *AIChE J.* **2022**, *68* (6), No. e17633.

(10) Nikita, S.; Mishra, S.; Gupta, K.; Runkana, V.; Gomes, J.; Rathore, A. S. Advances in Bioreactor Control for Production of Biotherapeutic Products. *Biotechnol. Bioeng.* **2023**, *120*, 1189−1214.

(11) Ranghetti, L.; Rivera, D. E.; Guo, P.; Visioli, A.; Savage Williams, J.; Symons Downs, D. A Control-Based Observer Approach for Estimating Energy Intake during Pregnancy. *Int. J. Robust Nonlinear Control* **2023**, *33* (9), 5105−5127.

(12) Myers, P. J.; Lee, S. H.; Lazzara, M. J. Mechanistic and Data-Driven Models of Cell Signaling: Tools for Fundamental Discovery and Rational Design of Therapy. *Curr. Opin. Syst. Biol.* **2021**, *28*, 100349.

(13) Verma, A.; Manchel, A.; Narayanan, R.; Hoek, J. B.; Ogunnaike, B. A.; Vadigepalli, R. A Spatial Model of Hepatic Calcium Signaling and Glucose Metabolism Under Autonomic Control Reveals Functional Consequences of Varying Liver Innervation Patterns Across Species. *Front. Physiol.* **2021**, *12*, 1935.

(14) Verma, B. K.; Subramaniam, P.; Vadigepalli, R. Modeling the Dynamics of Human Liver Failure Post Liver Resection. *Processes* **2018**, *6* (8), 115.

(15) Lee, D.; Jayaraman, A.; Kwon, J. S.-I. Identification of Cell-to-cell Heterogeneity through Systems Engineering Approaches. *AIChE J.* **2020**, *66* (5), No. e16925.

(16) Lee, D.; Singla, A.; Wu, H.-J.; Kwon, J. S.-I. An Integrated Numerical and Experimental Framework for Modeling of CTB and GD1b Ganglioside Binding Kinetics. *AIChE J.* **2018**, *64* (11), 3882−3893.

(17) Lee, D.; Jayaraman, A.; Sang-Il Kwon, J. Identification of a time-varying intracellular signalling model through data clustering and

parameter selection: application to NF- B signalling pathway induced by LPS in the presence of BFA. *IET Syst. Biol.* **2019**, *13* (4), 169−179.

(18) Mannino, D. M.; Buist, A. S. Global Burden of COPD: Risk Factors, Prevalence, and Future Trends. *Lancet* **2007**, *370* (9589), 765−773.

(19) GOLD. *Global Strategy For Prevention, Diagnosis And Management Of COPD: 2022 Report*; The Global Initiative for Chronic Obstructive Lung Disease (GOLD), 2022.

(20) Gao, C.; Taniguchi, N. Chronic Obstructive Pulmonary Disease (COPD). *Glycoscience: Biology and Medicine*; Springer Japan: Tokyo, 2015; pp 1267−1274.

(21) Halpin, D. M. G.; Celli, B. R.; Criner, G. J.; Frith, P.; López Varela, M.; Salvi, S.; Vogelmeier, C. F.; Chen, R.; Mortimer, K.; Montes de Oca, M.; et al. It Is Time for the World to Take COPD Seriously: A Statement from the GOLD Board of Directors. *Eur. Respiratory Soc.* **2019**, *54*, 1900914.

(22) Vogelmeier, C. F.; Román-Rodríguez, M.; Singh, D.; Han, M. K.; Rodríguez-Roisin, R.; Ferguson, G. T. Goals of COPD Treatment: Focus on Symptoms and Exacerbations. *Respir. Med.* **2020**, *166*, 105938.

(23) Franssen, F. M. E.; Alter, P.; Bar, N.; Benedikter, B. J.; Iurato, S.; Maier, D.; Maxheim, M.; Roessler, F. K.; Spruit, M. A.; Vogelmeier, C. F.; et al. Personalized Medicine for Patients with COPD: Where Are We? *Int. J. Chronic Obstruct. Pulm. Dis.* **2019**, *14*, 1465−1484.

(24) Kurian, V.; Ghadipasha, N.; Gee, M.; Chalant, A.; Hamill, T.; Okossi, A.; Chen, L.; Yu, B.; Ogunnaike, B. A.; Beris, A. N. Systems Engineering Approach to Modeling and Analysis of Chronic Obstructive Pulmonary Disease. *ACS Omega* **2023**, *8* (23), 20524−20535.

(25) Albanese, A.; Cheng, L.; Ursino, M.; Chbat, N. W. An Integrated Mathematical Model of the Human Cardiopulmonary System: Model Development. *Am. J. Physiol. Heart Circ. Physiol.* **2016**, *310* (7), H899−H921.

(26) Sarmiento, C. A.; Hernández, A. M.; Serna, L. Y.; Mañanas, M. Á. An Integrated Mathematical Model of the Cardiovascular and Respiratory Response to Exercise: Model-Building and Comparison with Reported Models. *Am. J. Physiol. Heart Circ. Physiol.* **2021**, *320* (4), H1235−H1260.

(27) Gutta, S.; Cheng, Q.; Nguyen, H. D.; Benjamin, B. A. Cardiorespiratory Model-Based Data-Driven Approach for Sleep Apnea Detection. *IEEE J. Biomed. Health Inf.* **2018**, *22* (4), 1036−1045.

(28) Abboud, S.; Barnea, O.; Guber, A.; Narkiss, N.; Bruderman, I. Maximum Expiratory Flow-Volume Curve: Mathematical Model and Experimental Results. *Med. Eng. Phys.* **1995**, *17* (5), 332−336.

(29) Bates, J. H. T. Systems Physiology of the Airways in Health and Obstructive Pulmonary Disease. *Wiley Interdiscip. Rev.: Syst. Biol. Med.* **2016**, *8* (5), 423−437.

(30) Jin, X.; Laxminarayan, S.; Nagaraja, S.; Wallqvist, A.; Reifman, J. Development and Validation of a Mathematical Model to Simulate Human Cardiovascular and Respiratory Responses to Battlefield Trauma. *Int. J. Numer. Method. Biomed. Eng.* **2023**, *39* (1), No. e3662.

(31) Kurian, V.; Ghadipasha, N.; Beris, A.; Ogunnaike, B. A. Effect of Metabolic Rates in the Modeling of the Cardio-Respiratory System in COPD Patients. *IFAC-PapersOnLine* **2022**, *55* (23), 41−45.

(32) Guyton, A.; Hall, J. *Textbook of Medical Physiology*, 11th ed.; Elsevier Inc. 2006.

(33) Tiwari, A.; Liaqat, S.; Liaqat, D.; Gabel, M.; de Lara, E.; Falk, T. H. Remote Copd Severity and Exacerbation Detection Using Heart Rate and Activity Data Measured from a Wearable Device. *2021 43rd Annual International Conference of the IEEE Engineering in Medicine & Biology Society (EMBC)*; IEEE, 2021.

(34) Calverley, P. M. A. Dynamic Hyperinflation: Is It Worth Measuring? *Proc. Am. Thorac. Soc.* **2006**, *3* (3), 239−244.

(35) Armstrong, M. J.; Beris, A. N.; Wagner, N. J. An Adaptive Parallel Tempering Method for the Dynamic Data-driven Parameter Estimation of Nonlinear Models. *AIChE J.* **2017**, *63* (6), 1937−1958.

(36) Jetté, M.; Sidney, K.; Blümchen, G. Metabolic Equivalents (METS) in Exercise Testing, Exercise Prescription, and Evaluation of Functional Capacity. *Clin. Cardiol.* **1990**, *13* (8), 555−565.

(37) Ben-Tal, A.; Smith, J. C. A Model for Control of Breathing in Mammals: Coupling Neural Dynamics to Peripheral Gas Exchange and Transport. *J. Theor. Biol.* **2008**, *251* (3), 480−497.

(38) Medicine, American College of Sports. *ACSM's Advanced Exercise Physiology*; Lippincott Williams & Wilkins, 2006; Vol. *143*.

(39) Batzel, J. J.; Kappel, F.; Schneditz, D.; Tran, H. T. *Cardiovascular and Respiratory Systems: Modeling, Analysis, and Control*; SIAM, 2007.

(40) Molkov, Y. I.; Shevtsova, N. A.; Park, C.; Ben-Tal, A.; Smith, J. C.; Rubin, J. E.; Rybak, I. A. A Closed-Loop Model of the Respiratory System: Focus on Hypercapnia and Active Expiration. *PLoS One* **2014**, *9* (10), No. e109894.

(41) Chiang, S. T.; Steigbigel, N. H.; Lyons, H. A. Pulmonary Compliance and Nonelastic Resistance during Treadmill Exercise. *J. Appl. Physiol.* **1965**, *20* (6), 1194−1198.

(42) Edwards, Z.; Annamaraju, P. Physiology, Lung Compliance. *StatPearls*; StatPearls Publishing: Treasure Island (FL), 2023.

(43) Sun, X.-G.; Hansen, J. E.; Garatachea, N.; Storer, T. W.; Wasserman, K. Ventilatory Efficiency during Exercise in Healthy Subjects. *Am. J. Respir. Crit. Care Med.* **2002**, *166* (11), 1443−1448.

(44) Vincent, J.-L. Understanding Cardiac Output. *Crit. Care* **2008**, *12*, 174−183.

(45) Borg, G.; Hassmén, P.; Lagerström, M. Perceived Exertion Related to Heart Rate and Blood Lactate during Arm and Leg Exercise. *Eur. J. Appl. Physiol. Occup. Physiol.* **1987**, *56*, 679−685.

(46) Pawelczyk, J. A.; Hanel, B.; Pawelczyk, R. A.; Warberg, J.; Secher, N. H. Leg Vasoconstriction during Dynamic Exercise with Reduced Cardiac Output. *J. Appl. Physiol.* **1992**, *73* (5), 1838−1846.

(47) Otsuki, T.; Maeda, S.; Iemitsu, M.; Saito, Y.; Tanimura, Y.; Ajisaka, R.; Miyauchi, T. Systemic Arterial Compliance, Systemic Vascular Resistance, and Effective Arterial Elastance during Exercise in Endurance-Trained Men. *Am. J. Physiol. Regul. Integr. Comp. Physiol.* **2008**, *295* (1), R228−R235.

(48) Wright, S. P.; Granton, J. T.; Esfandiari, S.; Goodman, J. M.; Mak, S. The Relationship of Pulmonary Vascular Resistance and Compliance to Pulmonary Artery Wedge Pressure during Submaximal Exercise in Healthy Older Adults. *J. Physiol.* **2016**, *594* (12), 3307−3315.

(49) Biselli, P.; Grossman, P. R.; Kirkness, J. P.; Patil, S. P.; Smith, P. L.; Schwartz, A. R.; Schneider, H. The Effect of Increased Lung Volume in Chronic Obstructive Pulmonary Disease on Upper Airway Obstruction during Sleep. *J. Appl. Physiol.* **2015**, *119* (3), 266−271.

(50) Chaouat, A.; Naeije, R.; Weitzenblum, E. Pulmonary Hypertension in COPD. *Eur. Respir. J.* **2008**, *32* (5), 1371−1385.

(51) Balakrishnan, N. P.; Samavedham, L.; Rangaiah, G. P. Personalized Mechanistic Models for Exercise, Meal and Insulin Interventions in Children and Adolescents with Type 1 Diabetes. *J. Theor. Biol.* **2014**, *357*, 62−73.

(52) Verma, N.; Verma, B. K.; Pushpavanam, S. Modeling Temperature-Dependent Sex Determination in Oviparous Species Using a Dynamical Systems Approach. *Bull. Math. Biol.* **2020**, *82*, 89.

(53) Pianosi, F.; Wagener, T. Distribution-Based Sensitivity Analysis from a Generic Input-Output Sample. *Environ. Model. Software* **2018**, *108*, 197−207.

(54) Gee, M. M.; Lenhoff, A. M.; Schwaber, J. S.; Ogunnaike, B. A.; Vadigepalli, R. Closed-loop Modeling of Central and Intrinsic Cardiac Nervous System Circuits Underlying Cardiovascular Control. *AIChE J.* **2023**, *69* (4), No. e18033.

(55) Park, J. H.; Gorky, J.; Ogunnaike, B.; Vadigepalli, R.; Schwaber, J. S. Investigating the Effects of Brainstem Neuronal Adaptation on Cardiovascular Homeostasis. *Front. Neurosci.* **2020**, *14*, 470.

(56) Tsallis, C.; Stariolo, D. A. Generalized Simulated Annealing. *Phys. A* **1996**, *233* (1−2), 395−406.

(57) Bittner, E.; Nußbaumer, A.; Janke, W. Make Life Simple: Unleash the Full Power of the Parallel Tempering Algorithm. *Phys. Rev. Lett.* **2008**, *101* (13), 130603.

(58) Metropolis, N.; Rosenbluth, A. W.; Rosenbluth, M. N.; Teller, A. H.; Teller, E. Equation of State Calculations by Fast Computing Machines. *J. Chem. Phys.* **1953**, *21* (6), 1087−1092.

(59) Sahimi, M.; Hamzehpour, H. Efficient Computational Strategies for Solving Global Optimization Problems. *Comput. Sci. Eng.* **2010**, *12* (4), 74−83.

(60) Zhang, Y.; Agnoletti, D.; Blacher, J.; Safar, M. E. Blood Pressure Variability in Relation to Autonomic Nervous System Dysregulation: The X-CELLENT Study. *Hypertens. Res.* **2012**, *35* (4), 399−403.

(61) Cain, P. A.; Ahl, R.; Hedstrom, E.; Ugander, M.; Allansdotter-Johnsson, A.; Friberg, P.; Arheden, H. Age and Gender Specific Normal Values of Left Ventricular Mass, Volume and Function for Gradient Echo Magnetic Resonance Imaging: A Cross Sectional Study. *BMC Med. Imag.* **2009**, *9* (1), 2.

(62) Holmgren, A.; Linderholm, H. Oxygen and Carbon Dioxide Tensions of Arterial Blood during Heavy and Exhaustive Exercise. *Acta Physiol. Scand.* **1958**, *44* (3−4), 203−215.

(63) Sharratt, M. T.; Henke, K. G.; Aaron, E. A.; Pegelow, D. F.; Dempsey, J. A. Exercise-Induced Changes in Functional Residual Capacity. *Respir. Physiol.* **1987**, *70* (1), 313−326.

(64) Jackson, H.; Hubbard, R. Detecting Chronic Obstructive Pulmonary Disease Using Peak Flow Rate: Cross Sectional Survey. *BMJ* **2003**, *327* (7416), 653−654.

(65) Madani, A.; Van Muylem, A.; Gevenois, P. A. Pulmonary Emphysema: Effect of Lung Volume on Objective Quantification at Thin-Section CT. *Radiology* **2010**, *257* (1), 260−268.

(66) Christensen, C. C.; Ryg, M. S.; Edvardsen, A.; Skjønsberg, O. Effect of Exercise Mode on Oxygen Uptake and Blood Gases in COPD Patients. *Respir. Med.* **2004**, *98* (7), 656−660.

(67) Alowiwi, H.; Watson, S.; Jetmalani, K.; Thamrin, C.; Johns, D. P.; Walters, E. H.; King, G. G. Relationship between Concavity of the Flow-Volume Loop and Small Airway Measures in Smokers with Normal Spirometry. *BMC Pulm. Med.* **2022**, *22* (1), 211−215.

(68) Guenette, J. A.; Chin, R. C.; Cory, J. M.; Webb, K. A.; O'Donnell, D. E. Inspiratory Capacity during Exercise: Measurement, Analysis, and Interpretation. *Pulm. Med.* **2013**, *2013*, 1−13.

(69) Guenette, J. A.; Webb, K. A.; O'Donnell, D. E. Does Dynamic Hyperinflation Contribute to Dyspnoea during Exercise in Patients with COPD? *Eur. Respir. J.* **2012**, *40* (2), 322−329.

(70) El Mistiri, M.; Khan, O.; Rivera, D. E.; Hekler, E. System Identification and Hybrid Model Predictive Control in Personalized MHealth Interventions for Physical Activity. *Proc. Am. Control Conf.* **2023**, *2023*, 2240−2245.

(71) Lee, D.; Jayaraman, A.; Kwon, J. S. Development of a Hybrid Model for a Partially Known Intracellular Signaling Pathway through Correction Term Estimation and Neural Network Modeling. *PLoS Comput. Biol.* **2020**, *16* (12), No. e1008472.

(72) Shah, P.; Sheriff, M. Z.; Bangi, M. S. F.; Kravaris, C.; Kwon, J. S.-I.; Botre, C.; Hirota, J. Deep Neural Network-Based Hybrid Modeling and Experimental Validation for an Industry-Scale Fermentation Process: Identification of Time-Varying Dependencies among Parameters. *Chem. Eng. J.* **2022**, *441*, 135643.

(73) Bangi, M. S. F.; Kao, K.; Kwon, J. S.-I. Physics-Informed Neural Networks for Hybrid Modeling of Lab-Scale Batch Fermentation for β-Carotene Production Using Saccharomyces Cerevisiae. *Chem. Eng. Res. Des.* **2022**, *179*, 415−423.

(74) Patel, N.; Kinmond, K.; Jones, P.; Birks, P.; Spiteri, M. A. Validation of COPDPredict: Unique Combination of Remote Monitoring and Exacerbation Prediction to Support Preventative Management of COPD Exacerbations. *Int. J. Chronic Obstruct. Pulm. Dis.* **2021**, *2021* (16), 1887−1899.

(75) Wu, C.-T.; Li, G.-H.; Huang, C.-T.; Cheng, Y.-C.; Chen, C.-H.; Chien, J.-Y.; Kuo, P.-H.; Kuo, L.-C.; Lai, F. Acute Exacerbation of a Chronic Obstructive Pulmonary Disease Prediction System Using Wearable Device Data, Machine Learning, and Deep Learning: Development and Cohort Study. *JMIR mHealth and uHealth* **2021**, *9* (5), No. e22591.

(76) Coleman, J. M.; Wolfe, L. F.; Kalhan, R. Noninvasive Ventilation in Chronic Obstructive Pulmonary Disease. *Ann. Am. Thorac. Soc.* **2019**, *16* (9), 1091−1098.

(77) Wagner, P. D. Pulmonary Gas Exchange. In *An Introductory Text To Bioengineering*; Chien, S., Chen, P. C., Fung, Y. C., Eds.; World Scientific, 2008.

(78) Ben-Tal, A. Simplified Models for Gas Exchange in the Human Lungs. *J. Theor. Biol.* **2006**, *238* (2), 474−495.

(79) Ellwein, L. M.; Pope, S. R.; Xie, A.; Batzel, J. J.; Kelley, C. T.; Olufsen, M. S. Patient-Specific Modeling of Cardiovascular and Respiratory Dynamics during Hypercapnia. *Math. Biosci.* **2013**, *241* (1), 56−74.

(80) *MATLAB, Variable Transport Delay*, 2020.

(81) Kwon, Y.; Mariani, S.; Gadi, S. R.; Jacobs Jr, D. R.; Punjabi, N. M.; Reid, M. L.; Azarbarzin, A.; Wellman, A. D.; Redline, S. Characterization of Lung-to-Finger Circulation Time in Sleep Study Assessment: The Multi-Ethnic Study of Atherosclerosis. *Physiol. Meas.* **2020**, *41* (6), 065004.

(82) Caruana-Montaldo, B.; Gleeson, K.; Zwillich, C. W. The Control of Breathing in Clinical Practice. *Chest* **2000**, *117* (1), 205−225.

(83) Ramirez, J.-M.; Richter, D. W. The Neuronal Mechanisms of Respiratory Rhythm Generation. *Curr. Opin. Neurobiol.* **1996**, *6* (6), 817−825.

(84) Butera, R. J.; Rinzel, J.; Smith, J. C. Models of Respiratory Rhythm Generation in the Pre-Botzinger Complex. I. Bursting Pacemaker Neurons. *J. Neurophysiol.* **1999**, *82* (1), 382−397.

(85) Rybak, I. A.; Paton, J. F. R.; Schwaber, J. S. Modeling Neural Mechanisms for Genesis of Respiratory Rhythm and Pattern. I. Models of Respiratory Neurons. *J. Neurophysiol.* **1997**, *77* (4), 1994−2006.

(86) Milhorn, H. T.; Benton, R.; Ross, R.; Guyton, A. C. A Mathematical Model of the Human Respiratory Control System. *Biophys. J.* **1965**, *5* (1), 27−46.

(87) Holland, R. A.; Forster, R. E. Effect of Temperature on Rate of CO2 Uptake by Human Red Cell Suspensions. *Am. J. Physiol.* **1975**, *228* (5), 1589−1596.

(88) McKeever, T. M.; Weston, P. J.; Hubbard, R.; Fogarty, A. Lung Function and Glucose Metabolism: An Analysis of Data from the Third National Health and Nutrition Examination Survey. *Am. J. Epidemiol.* **2005**, *161* (6), 546−556.

(89) Christie, C. R.; Achenie, L. E. K.; Ogunnaike, B. A. A Control Engineering Model of Calcium Regulation. *J. Clin. Endocrinol. Metab.* **2014**, *99* (8), 2844−2853.

(90) Ainsworth, B. E.; Haskell, W. L.; Leon, A. S.; Jacobs, D. R.; Montoye, H. J.; Sallis, J. F.; Paffenbarger, R. S. Compendium of Physical Activities: Classification of Energy Costs of Human Physical Activities. *Med. Sci. Sports Exerc.* **1993**, *25* (1), 71−80.